Langmuir
Article
pubs.acs.org/Langmuir
© 2010 American Chemical Society

Controlled Production of Droplets by In-Flight Electrospraying

Oleg V. Kim*,† and Patrick F. Dunn*

Particle Dynamics Laboratory, Department of Aerospace and Mechanical Engineering, University of Notre Dame, Notre Dame, Indiana 46556. †Current address: Particle Dynamics Laboratory, Department of Aerospace and Mechanical Engineering, Notre Dame, University of Notre Dame, Indiana 46556.

Received July 13, 2010. Revised Manuscript Received August 24, 2010

Diameter, velocity, and charge measurements of progeny droplets produced in-flight by a millimeter-size parent drop subjected to electric and ionic fields are reported. Different drop breakup modes were studied using phase doppler anemometry and high-speed digital photography. Drop breakup occurred in applied electric (~1 kV/cm to ~10 kV/cm) and ionic (~10^{13}/m^3 to ~10^{15}/m^3) fields that were generated using a DC-corona discharge in a needle−plate configuration. Effects of the external electric field and the diameter of the parent drop are considered. Several models are summarized, including simulations of the electrohydrodynamics of the corona discharge, electrocapillary stability analysis of the jet, and progeny droplets mobility analysis. Using experimental and model results, the charge of progeny drops is shown to vary as the three-halves power of their diameter.

Introduction

This work was motivated by the need to develop a novel, simple, and controllable method to produce electrically charged droplets (from micrometer-size to nanometer-size) from larger (millimeter-size) electrically neutral drops. The developed method can be used in a variety of applications. For example, in air filtration, charged nanometer-size water droplets can be utilized to charge and help to collect airborne impurities. In biotechnology, single molecular structures can be encapsulated in a liquid, separated according to size, and then directed to a specific target. The fundamental science behind this method relates to the behavior of an electrically charged drop and its surface stability in an external electric field. This is part of research areas in atmospheric science, aerosol technology, combustion, mass spectroscopy, and instrumentation.[1−5]

Although there are a number of experimental studies on charge and mass loss of an unstable *parent* drop experiencing Rayleigh discharge,[6−9] few charge and size measurements of *progenies* have been performed. Studies have been made by Hunter and Ray[10] and by Li et al.,[11] in which the size of progenies was determined indirectly from the measured mass and charge losses of the parent drop. These losses, in turn, were obtained from experimental scattering intensities. The only reported study in which progeny size was measured directly is that of Gomez and Tang.[12] Using a phase Doppler anemometry (PDA) system, they measured the size and velocities of offspring droplets produced in electrostatic sprays. However, no information was presented on progeny size distributions produced by an individual drop. How progenies are produced from parent drops when experiencing sub-Rayleigh or Rayleigh instabilities and how they are distributed in size and charge remain intriguing questions. Experimental data on these are lacking.

Little attention has been given to charged drop breakup subjected to an electric field when accompanied by a simultaneous charge transfer toward the drop surface. Hager et al.[4] reported the use of corona-discharge-droplet charging for electrospray mass spectrometry. In their study, the focus was on mass spectra observed when 16 and 21 μm droplets of acetone produced a spray of smaller progenies as they evaporated. No information was given about droplet formation per se and on progeny size and charge characterization.

Direct and indirect charge measurements of drops passing through the corona region were done by Kim and Dunn.[13] In their experiments, drops experiencing electric stresses oscillated but did not break up and produce progenies.

In this paper, the characteristics of progeny droplets produced by an individual ethanol parent drop subjected in-flight to ionic and electric fields are studied experimentally. High-speed digital photography and a PDA system were used to measure the size and velocity of progeny droplets. The charge of progenies subsequently was determined using mobility analysis. The presented results are new and have not appeared in the literature. These provide further insight into the nature of charged drop behavior.

Experimental Section

A schematic of the general experimental setup is shown in Figure 1. The parent drop was generated through the blunt-tip needle, connected with 1.5 m tubing to the liquid reservoir. The pump was used to pressurize the reservoir to 2 psig (~14 kPa gage) to achieve the constant drop production rate of 3 drops/s. The traverse system was used to accurately control the position of the laser. The applied voltage difference, U_{app}, was controlled by a high-voltage negative-DC power supply and

*To whom correspondence should be addressed. E-mail: okim@nd.edu (O.V.K.); pdunn@nd.edu (P.F.D.).

(1) Koromyslov, V. A.; Grigor'ev, A. I. *Tech. Phys.* **2002**, *47*, 1090–1097.
(2) Bologa, A.; Paur, H.-R.; Seifert, H.; Woletz, K. *J. Electrost.* **2009**, *67*, 150–153.
(3) Tao, R.; Huang, K.; Tang, H.; Bell, D. *Energy Fuels* **2008**, *22*, 3785–3788.
(4) Hager, D. B.; Dovichi, N. J.; Klassen, J.; Kebarle, P. *Anal. Chem.* **1994**, *66*, 3944–3949.
(5) Grimm, R. L.; Beauchamp, J. L. *J. Phys. Chem. B* **2003**, *107*, 14161–14163.
(6) Giglio, E.; Gervais, B.; Rangama, J.; Manil, B.; Huber, B. A.; Duft, D.; Muller, R.; Leisner, T.; Guet, C. *Phys. Rev. E* **2008**, *77*, 036319.
(7) Grimm, R. L.; Beauchamp, J. L. *J. Phys. Chem. B* **2005**, *109*, 8244–8250.
(8) de Juan, L.; de la Mora, J. F. *J. Colloid Interface Sci.* **1997**, *186*, 280–293.
(9) Richardson, C. B.; Pigg, A. L.; Hightower, R. L. *Proc. R. Soc. London, Ser. A* **1989**, *422*, 319–328.
(10) Hunter, H. C.; Ray, A. K. *Phys. Chem. Chem. Phys.* **2009**, *11*, 6156–6165.
(11) Li, K.-Y.; Tu, H. H.; Ray, A. K. *Langmur* **2005**, *21*, 3786–3794.
(12) Gomez, A.; Tang, K. *Phys. Fluids* **1994**, *6*, 404–414.
(13) Kim, O. V.; Dunn, P. F. *Aerosol Sci. Technol.* **2010**, *44*, 292–301.

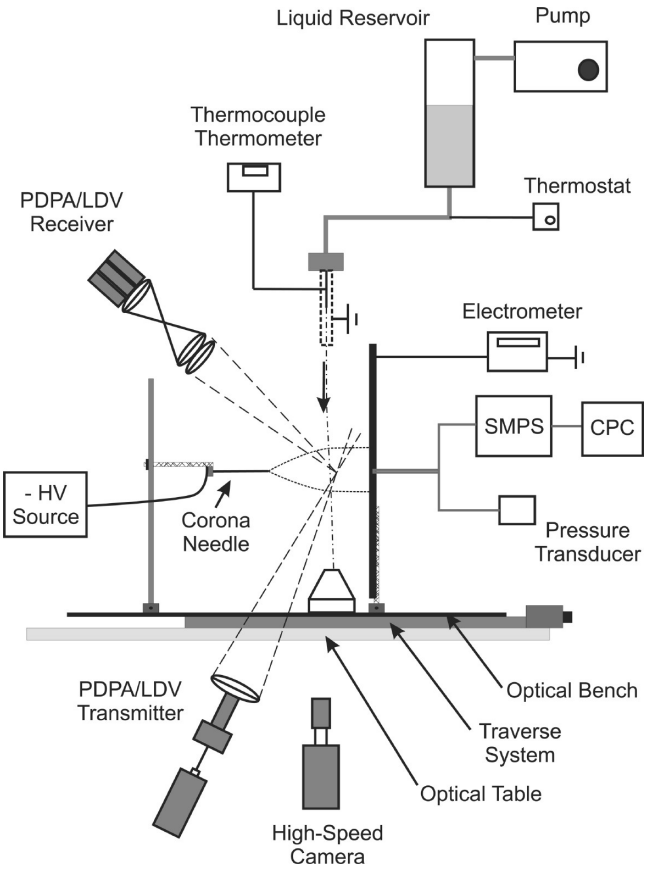

Figure 1. Schematic of the experimental setup.

varied from 0 to 50 kV in steps of either 1 or 2 kV. A 23-gauge hypodermic needle was used as a corona electrode placed at L_0 = 5.6 cm from the 35 cm × 45 cm grounded plate. The liquid-feed system, all measurement equipment, the optical table, as well as all holders, mounts, and tripods were grounded electrically in order to avoid an unwanted accumulation of static charges. Additional shielding of the liquid-feed needle was taken to eliminate induced chargers on a drop at the moment of pinch-off at the needle tip. The feeding needle shield was a circular copper cylinder having a diameter of 10.4 mm and a length of 10.3 cm.

In experiments, millimeter-diameter parent drops emanated from the blunt-tip needle, which was placed at 30 cm above from the corona needle axis. Due to an electrocapillary instability of the surface of the drop induced via corona discharge by electric and hydrodynamic stresses, the moving parent drop started to deform and break up into a number of smaller progeny droplets. The production of progenies was accompanied by the formation of a transient cone-jet structure. The jet extended out of the drop apex and broke up into charged droplets. Depending on the applied electric field strength, different modes of the jet breakup occurred.

The diameter and the velocity of progeny droplets were measured using a PDA system. The size distribution function and the velocity−diameter correlation of progeny droplets were measured for three different diameters of the parent drop (1.89, 2.10, and 2.21 mm), for two parent-drop initial positions (0.5 and 1 cm), and for various applied voltage differences across the needle−plate gap (33−50 kV). This was done to study the effect of the size of the parent drop and the strength of the electric field on the size of produced progeny droplets. Before progeny drop measurements, the PDA system was calibrated and the size of the parent drop was measured using high-speed digital photography.

Figure 2 shows overlaid images of a parent drop dynamics when the applied voltage difference varies from 0 to 50 kV. It is clearly seen that as the applied electric field increases, the drops deflect to larger angles. The increase of electric stresses results in

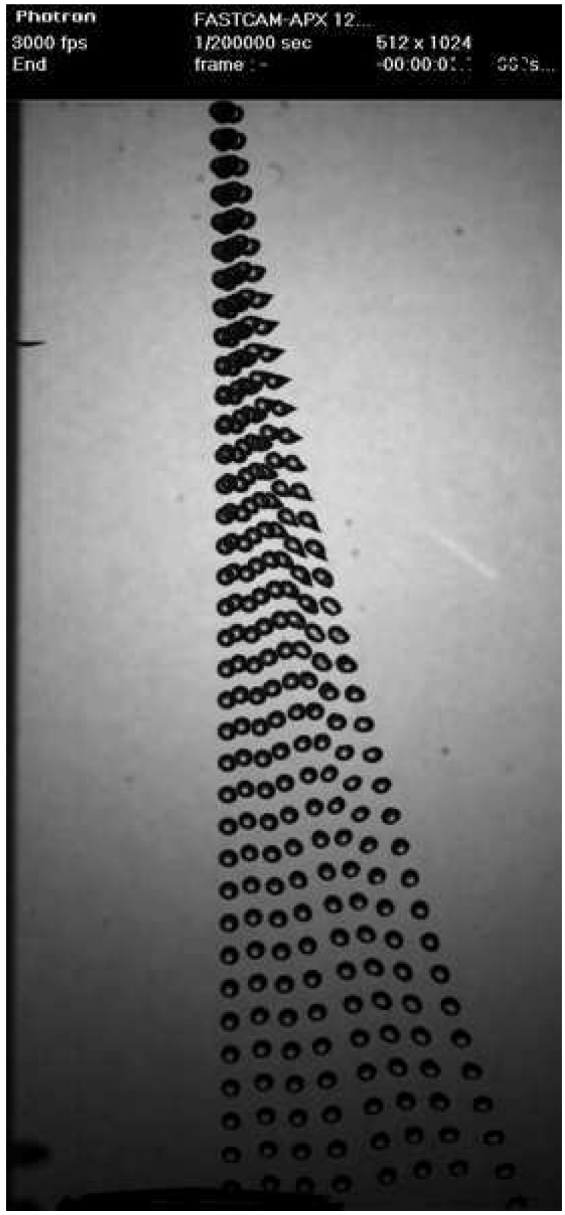

Figure 2. Parent drop trajectories at various applied voltage differences (0−50 kV). The distance between the tip of the corona needle and the grounded electrode was 8 cm. The initial drop diameter was 2.21 mm.

stronger deformations, which change the spherical shape of the drop to egg-or tear-shape, having the higher curvature on the side carrying the net charge. At some critical electric field, this shape becomes unstable. The jet is formed at the drop apex and breaks up into progenies.

The progeny-drop measurement positions and electrode configuration are shown schematically in Figure 3. Here, the origin of the z-axis is at the tip of the corona needle. The coordinate z_d is the position of the parent drop, z_p is the position of the laser, and Δz_p = 2 mm is the step between laser positions. Diameter and velocity data were collected at 10 different positions from the spraying parent drop. The first measurement position of the laser, z_1, was 1.6 cm when z_d^0 = 0.5 and 2.2 cm when z_d^0 = 1 cm. The liquid was ethanol with ρ (density) = 789 kg/m^3, μ (absolute viscosity) = 1.17 mPa·s, σ (surface tension) = 0.023 N/m, ε_r (relative permeability) = 21, and K (conductivity) = 0.4 mS/m. The effect of the applied voltage difference on the produced size distribution and velocity−diameter correlation of progeny drops was investigated.

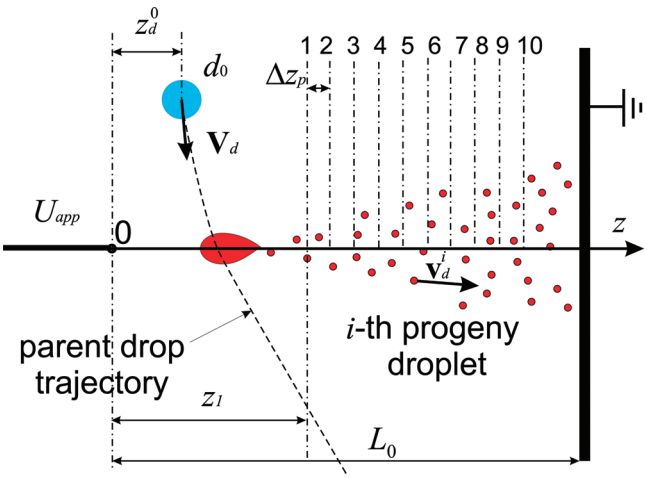

Figure 3. Schematic of the progeny measurements experiment. PDA measurements were done along the z-axis (z_d^0 = 10 mm, z_1 = 22 mm; z_d^0 = 5 mm, z_1 = 16 mm; Δz_p = 2 mm).

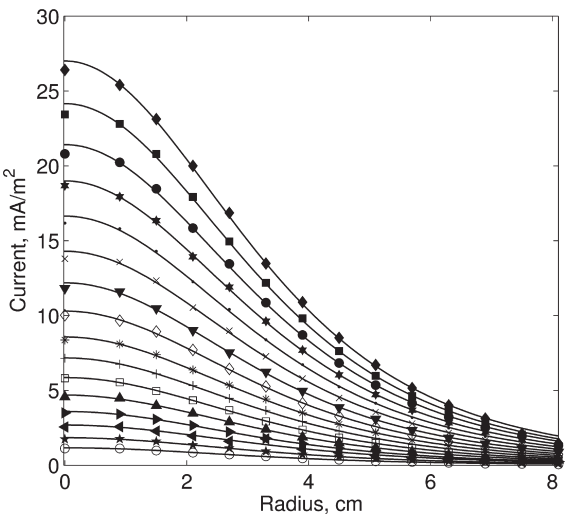

Figure 4. Measured current density distribution for L_0 = 5.6 cm. Symbols indicate various applied potential differences; lines show power-law fits. The lowest curve and open circles, U_{app} = 10 kV; the highest curve and solid diamonds, U_{app} = 40 kV. The applied voltage for each successive curve differs from the preceding curve by 2 kV.

In order to determine electric and aerodynamic forces acting on progeny droplets, experimental and numerical studies of corona discharge were performed. Corona current measurements were done for the needle-to-plate configuration shown in Figure 3 to identify the appropriate boundary conditions for the grounded electrode. These measurements included current−density distribution measurements on the grounded plate and total current versus voltage measurements for the applied voltage range from 0 to 45 kV. A Keithley electrometer was used to measure the current in the range from nA to μA. In order to measure the current density, the grounded plate was divided into 14 circular conducting segments of 5 mm width, excluding the central segment, which had the radius of 5.4 mm. The current through each segment was measured from 0 to 45 kV, and the corresponding averaged current density was obtained by dividing the current over the electrode surface area.

Results and Discussion

Corona Discharge Measurements. Figure 4 shows the obtained current density distributions as a function of the radial coordinate, with different symbols corresponding to various applied voltage differences. The solid lines depict the power-law fits given by Warburg's law[14,15]

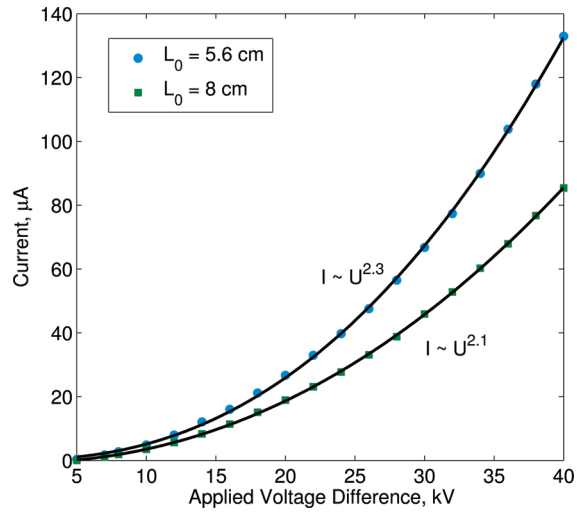

Figure 5. Measured current−voltage characteristics for L_0 = 5.6 cm and L_0 = 8 cm.

$$j_{\mathrm{fit}} = a_j\left(L_0/\sqrt{L_0^2+r^2}\right)^{b_j} \tag{1}$$

where the coefficients a_j and b_j are the fitting coefficients and L_0 = 5.6 cm. These approximations were used to impose boundary conditions on the grounded electrode in the corona discharge model. The current−voltage characteristics of a corona discharge are shown in Figure 5, clearly revealing a parabolic dependence of the corona discharge current on the applied voltage difference.

Corona Discharge Simulation. In order to find a progeny charge, the electric field strength, the velocity field, and their distributions were determined numerically using the electrohydrodynamic model of the corona discharge.

The motion of an ionized gas is described by a system of electrohydrodynamic equations. It consists of the conservation of mass

$$\frac{D\rho_g}{Dt}+\rho_g\nabla\cdot\mathbf{V}_g = 0 \tag{2}$$

and the Navier−Stokes equations, accounting for the body force

$$\rho_g\frac{D\mathbf{V}_g}{Dt} = -\nabla p+\mu_g\Delta\mathbf{V}_g+\rho_i\mathbf{E} \tag{3}$$

Here, D/Dt denotes the total derivative, $\mathbf{V}_g$ is the gas velocity, ρ_g is the gas density, μ_g is the gas absolute viscosity, ρ_i is the volume charge, $\mathbf{E}$ is the applied electric field vector, p is the reduced pressure, and ∇ denotes the Laplacian operator. It is assumed that the internal ionization region can be neglected and that unipolar electric charges are ejected from the surface of the corona electrode. Based on these assumptions, the governing equations for the electric field of the corona discharge are the Poisson

$$\Delta\phi_E = -\rho_i/\varepsilon_g \tag{4}$$

and the charge conservation equations

$$\nabla\cdot\mathbf{j} = 0 \tag{5}$$

(14) Warburg, E. *"Über die Spitzenentladung"*, Annalen der Physik und Chemie, **1899**, *67*, 69−83.
(15) Thomson, J. J.; Thomson, G. P. *Conduction of electricity through gases*, 3rd ed.; London: Cambridge University Press, 1933.

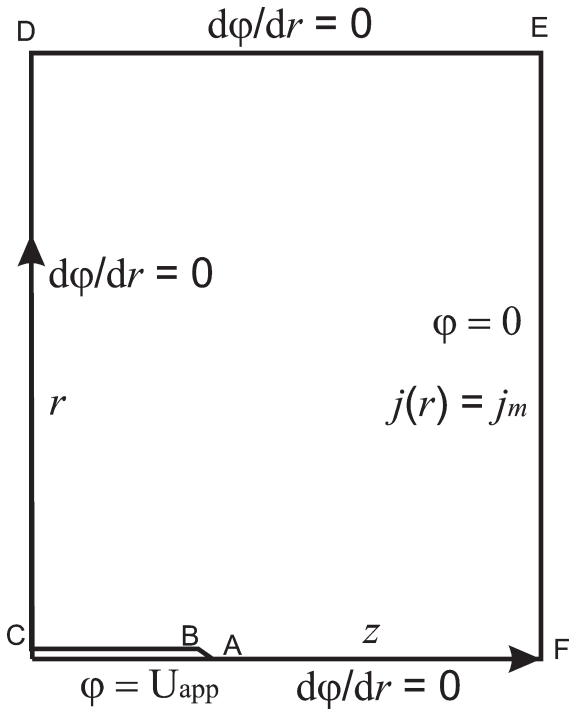

Figure 6. Simulation domain with boundary conditions.

where the electric field vector, **E**, and the current density vector, **j**, are defined as

$$\mathbf{E} = -\nabla\phi_{\mathrm{E}} \tag{6}$$

and

$$\mathbf{j} = k_{\mathrm{g}}\mathbf{E} + \rho_{\mathrm{e}}(\mu_i\mathbf{E} + \mathbf{V}_{\mathrm{g}}) - D_i\nabla\rho_i \tag{7}$$

Here, μ_{i} is the ion mobility ($=2 \times 10^{-4}$ V/(m^2 s)), k_{g} is the air conductivity ($\approx$0), ε_{g} is the permittivity of air ($\approx\varepsilon_0$), and ϕ_{E} is the potential of the external electric field. The convective, $j_{\mathrm{c}} \sim \rho_i V_{\mathrm{g}}$, as well as diffusive, $j_{\mathrm{diff}} \sim D_i\rho_i/L_0$, transports can be neglected when compared to the drift current density, $j_{\mathrm{dr}} \sim \rho_i\mu_i E$.

The simulation domain is shown in Figure 6. The following boundary conditions are imposed for ϕ_{E}:

$$\phi_{\mathrm{E}}|_{\mathrm{ABC}} = U_{\mathrm{app}} \tag{8}$$

$$\phi_{\mathrm{E}}|_{\mathrm{EF}} = 0 \tag{9}$$

and

$$\frac{\partial\phi_{\mathrm{E}}|_{\mathrm{CD,\,DE,\,AF}}}{\partial r} = 0 \tag{10}$$

where U_{app} is a known potential at the corona needle surface with respect to the grounded electrode. The Kaptsov hypothesis[16] is adopted, which suggests that maximum electric field on the surface of the corona electrode is given by the experimental Peek's value,[17]

$$E_0 = 31\delta\left[1 + \frac{0.0308}{\sqrt{0.5\delta r_0}}\right] \tag{11}$$

where $\delta = 1$ for normal conditions and $r_0 = 0.01$ cm is the radius of the needle electrode.

(16) Kaptsov, N. A. *Electric phenomena in gas and vacuum*, 1st ed.; Gostekhizdat: Moscow, 1950; pp 602−618.
(17) Peek, F. W. *Dielectric Phenomena in High Voltage Engineering*; McGraw-Hill Book Company, Inc.: New York, 1929.

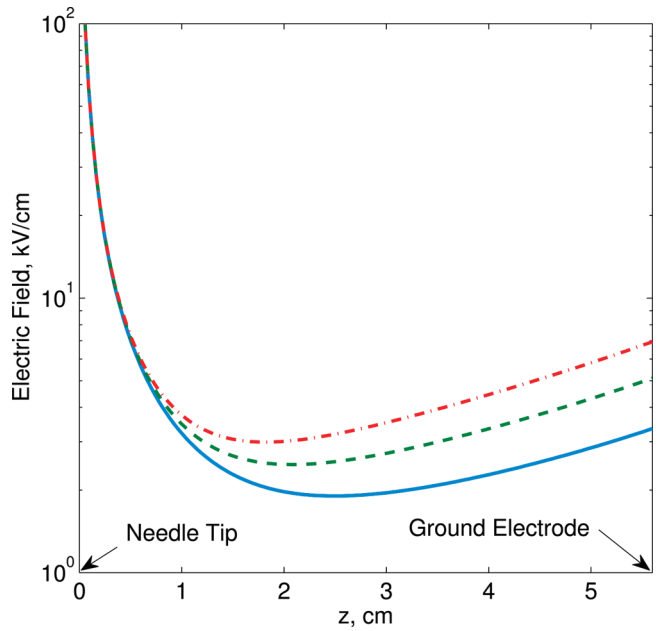

Figure 7. Modeled corona discharge electric field distribution along the z-axis. Solid line, $U_{\mathrm{app}} = 20$ kV; dashed line, $U_{\mathrm{app}} = 30$ kV; dot-dashed line, $U_{\mathrm{app}} = 40$ kV.

For the volume charge ρ_{i}, the following boundary condition is imposed

$$\rho_i^{\mathrm{EF}} = \rho_{\mathrm{m}} \tag{12}$$

Here, $\rho_{\mathrm{m}} = j_{\mathrm{m}}/(\mu_{\mathrm{i}}E_{\mathrm{EF}})$, where j_{m} is a measured current density distribution on the grounded plate electrode.

The boundary conditions for the airflow are straightforward. No-slip boundary conditions are imposed on the surfaces of the two electrodes. The sidewalls are defined as pressure outlet, because the computational domain is open in these areas and air is allowed to flow through these boundaries.

Figure 7 shows the distribution of the electric field in the gap between the corona needle and the grounded plate for different applied voltage differences. As seen from the figure, the presence of the volume charge increases the electric field in the vicinity of the grounded electrode. This is in accordance with studies given by Kozlov and Solov'ev[18] and also by Atten et al.[19]

The flow modeling results for $U_{\mathrm{app}} = 30$ kV are presented in Figure 8, which shows the stream line and the air velocity magnitude field. It is seen that a jet flow is induced by a body force toward the plate surface. The jet impacts the plate at a right angle and is deflected immediately, moving radially outward along the grounded plate surface. As seen from the velocity contour plot, due to radial spread of the impinging jet, the wall flow decelerates significantly as it travels downstream. The pressure gradient results in reversed flow vortices that are formed at approximately 20 cm from the flow symmetry line. These vortical structures are clearly distinguished by a closed streamline pattern.

Electric and velocity fields were modeled for different values of the applied voltage difference, U_{app}. These electrohydrodynamic parameters of the corona discharge were used in the mobility analysis of progeny droplets to determine their charge.

(18) Kozlov, B. A.; Solov'ev, V. I. *Tech. Phys.* **2009**, *5*, 621–630.
(19) Atten, P.; Adamiak, K.; Khaddour, B.; Coulomb, J.-L. *J. Optoelectron. Adv. Mater.* **2004**, *3*, 1023–1028.

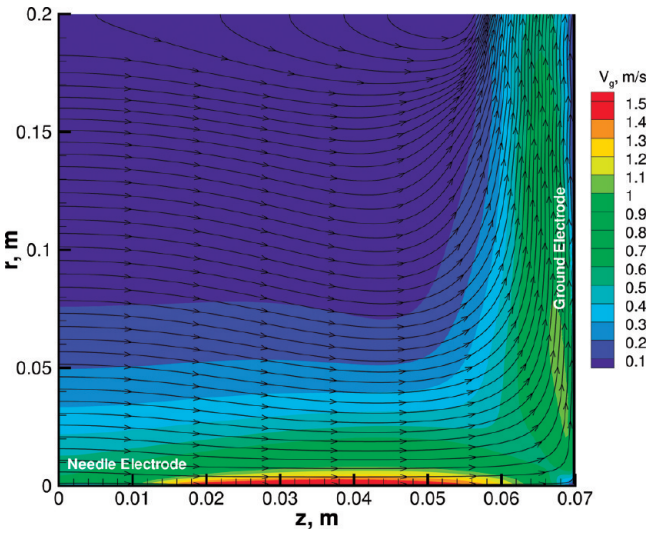

Figure 8. Modeled air flow induced by a corona discharge. Velocity magnitude contours and flow stream line pattern are shown for $U_{app} = 15$ kV and $L_0 = 5.6$ cm.

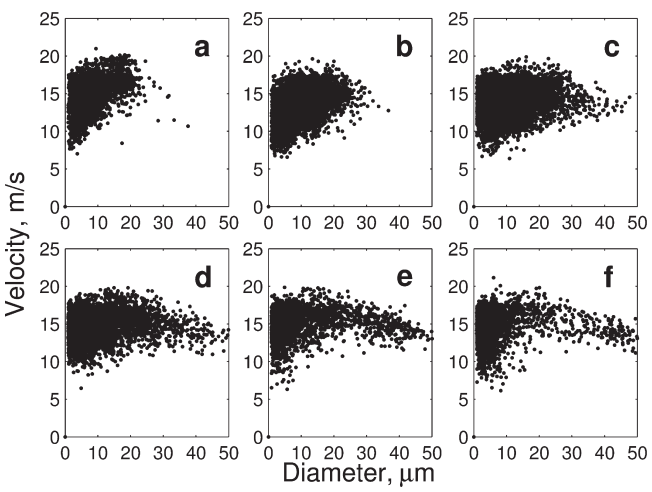

Figure 9. Velocity−diameter correlation of progeny drops as a function of applied voltage difference for $d_0 = 2.24$ mm, $z_d^0 = 1$ cm, and $z_p = 2.2$ cm. (a) $U_{app} = 34$ kV, (f) $U_{app} = 44$ kV. The step between each data set is 2 kV.

Progeny Size and Velocity Measurements. Figures 9 and 10 show velocity−diameter correlations and corresponding distribution functions for the 2.24 mm diameter parent drop when $z_d^0 = 1$ cm and $z_p = 22$ mm. The voltage difference was varied from 33 to 45 kV. When U_{app} was less than 38 kV, mostly monodisperse drops were produced from varicose jet breakup (Figure 11). The progeny were within the diameter−velocity domain of D_{dv} (1−25 μm; 8−19 m/s). As U_{app} increased, the electric stress on the drop surface also increased and higher modes of the jet became exited. When the applied voltage difference reached 39 kV, wider disperse drops appeared as the whipping breakup mode began (Figure 12). Consequently, the concentration of the droplets having a diameter greater than 22 μm increased (Figure 10). From $U_{app} = 41$ kV, the ramified breakup mode (Figure 13) developed, the number of larger droplets diminished, and the distribution moved toward smaller diameters. When U_{app} reached 44 kV, the increased electric field resulted in an instability of the produced progeny droplets. This produced a second generation of smaller progenies, which shifted the distribution toward the submicrometer and nanometer diameter range. The progeny data became

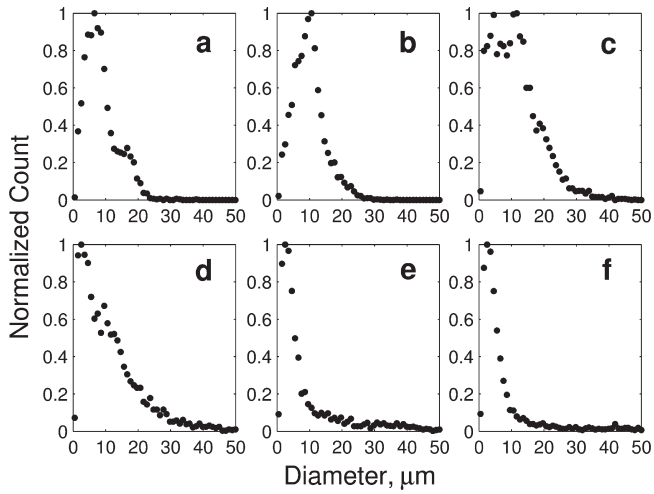

Figure 10. Size distribution function of progeny drops as a function of applied voltage difference for $d_0 = 2.24$ mm, $z_d^0 = 1$ cm, and $z_p = 2.2$ cm. (a) $U_{app} = 34$ kV, (f) $U_{app} = 44$ kV. The step between each data set is 2 kV.

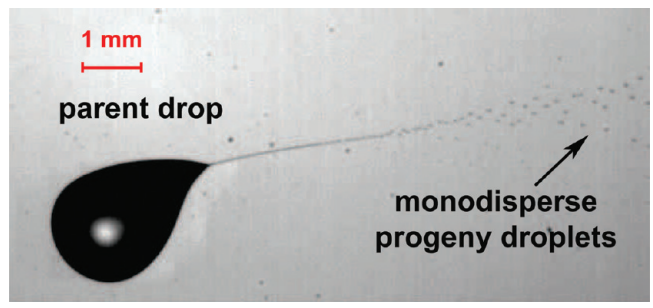

Figure 11. Varicose break-up mode of the jet emanating from the parent drop, $m = 0$.

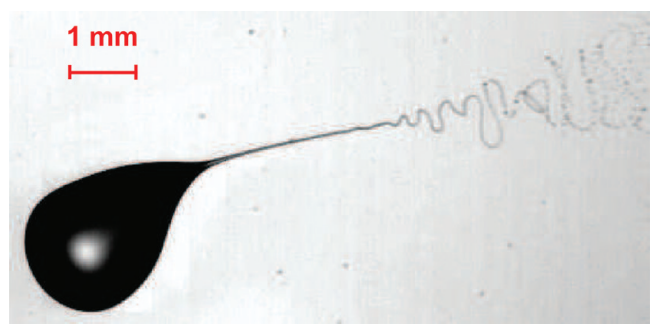

Figure 12. Lateral whipping break-up mode of the jet emanating from the parent drop, $m = 1$.

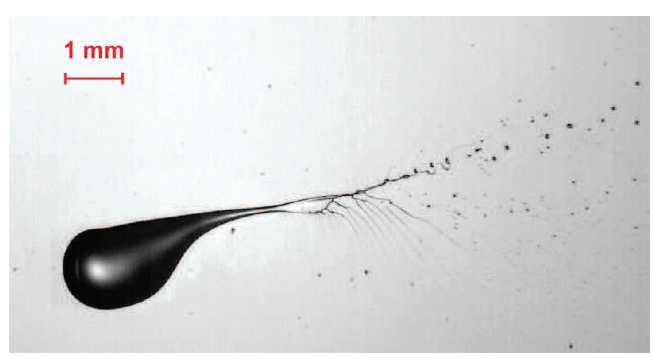

Figure 13. Ramified break-up mode of the jet emanating from the parent drop, $m = 2$.

distributed over the larger velocity−diameter domain, which, at 45 kV, had the diameter−velocity domain of D_{dv} (1−50 μm; 5.5−21 m/s). The diameter of submicrometer drops was not measured directly because of the low-detection limit (1 μm) of the PDA system.

The size distribution of progeny droplets depends upon the specific jet breakup mechanism. Depending on the electric to liquid surface stress ratio on the jet, different modes can be excited, which governs the formation of progenies. As this ratio grows, higher modes of instability may be excited with growth rates larger than that of the varicose mode.[20] As a result, more polydisperse droplets may form. The breakup of progeny droplets and formation of secondary progenies during the jet breakup in a ramified mode occurs because of the progeny surface electro-capillary instability. In addition to electric field of the corona discharge, the field of the strongly charged jet induces electric stresses, which assists in destabilizing progenies.

Using the results of the electrohydrodynamic model for the corona discharge and the experimental data from high-speed imaging, the instance of the parent drop spraying instability onset was determined. The drop began to spray when $\tilde{E} = E/E_T \sim 0.8-0.9$, $\tilde{q} = q_f/q_R \sim 0.5-0.6$, $s = a/b \sim 1.44$, and $We_d \sim 2.1-3.5$, when U_{app} varied from 30 to 45 kV. Here, a and b are the drop semiaxes, $E_T = c/(8\pi)^{1/2}(2\sigma/(\varepsilon_0 r))^{1/2}$ is the Taylor limit for a liquid droplet in air ($c = 1.625$), $q_f = 3\pi D^2\varepsilon_0 E\varepsilon_r/(\varepsilon_r + 2)$ is the field charging limit, $q_R = \pi(8\varepsilon_0\sigma D^3)^{1/2}$ is the Rayleigh limit, and $We_d = (\rho_g \Delta V_d^2 D)/\sigma$ is the parent drop Weber number, where D is the diameter of the parent drop. The parent drop Reynolds number, $Re_d = \rho_g \Delta V_d D/\mu_g$, ranged from 614 to 788. The values of E, q_f, and $\Delta V_d = |V_d - V_g|$ were determined at the location of the drop. It should be noted that the real charge of the parent drop is lower than the field limit q_f. Numerical simulations of the parent drop dynamics in the corona region showed[21] that $q \approx 0.7q_f$ to $0.85q_f$.

The drop spraying modes can be indirectly characterized in terms of the nondimensional flow rate through the jet, $\tilde{Q} = Q/Q^*$, where $Q^* = \sigma\tau_e/\rho = 0.8\ \mu$L/min and $\tau_e = \varepsilon_r\varepsilon_0/K = 0.5\ \mu$s is the charge relaxation time. The varicose jet breakup mode was observed when $1 < \tilde{Q}_{m=0} < 10^3$, the whipping mode when $10^3 < \tilde{Q}_{m=1} < 10^5$, and the ramified mode when $\tilde{Q}_{m=2} > 10^5$. It should be mentioned that, for in-flight electrospraying, the liquid flow rate is governed by the external electric field, which is different from the conventional electrospraying, where the flow rate is an independent parameter. How Q depends on the electric stresses on the individual drop is a subject of future study.

An analogy between a cone-jet formed on a drop and on a supported meniscus has been used[22] to predict the diameter of the jet and the progenies, when varicose and whipping modes occurred. The scaling laws for a steady cone-jet of a polar liquid yield the diameter of the jet $d_j = (Q\tau_e)^{1/3}$ and the diameter of progeny droplets $d = G(\varepsilon_r)(Q\tau_e)^{1/3}$. Here, Q is the flow rate through the cone and $G(\varepsilon_r) \approx 0.7$, as given by Loscertales and de la Mora.[23] The flow rate Q is not known a priori. Assuming $Q = Q_{min} = Q^* \sim \sigma\tau_e/\rho$ gives $d_{jet} \sim 1.8\ \mu$m and $d \sim 1.3\ \mu$m. Experimental mean values for progeny diameters obtained in the presented experiments were from 5 to 13 μm, which are within an order of magnitude of the predicted values.

One of the sources of an order of magnitude discrepancy is the used flow rate value $Q = Q_{min}$. From the experimental data, the flow rate was assessed to be of the order of from 10^{-8} to 10^{-6} m^3/s, which gave estimates of the mean droplet diameter from 10 to 50 μm, respectively. Thus, although the model was derived for the steady cone-jet mode, it can be used to estimate progeny sizes when the transient cone-jet structure on the parent drop occurs.

Progeny Charge Determination. The charge of the produced progenies was found from the growth rate measurements of the exited modes of the jet and using progeny mobility analysis.

By measuring the wavenumber, $k = 2\pi/\lambda$, of the unstable nonaxisymmetric mode, $m = 1$, and the jet diameter d_j, the value of the electric stress and the surface charge density on the jet was found by solving equation

$$\frac{\partial\tilde{\alpha}}{\partial\tilde{k}} = 0 \tag{13}$$

where $\tilde{\alpha}$ is the nondimensional growth rate and $\tilde{k} = kr_0$ is the nondimensional wavenumber. Assuming that $\lambda \gg r_0$, where r_0 is the jet radius, the dispersion equation for $\tilde{\alpha}$ can be written as[24,25]

$$\tilde{\alpha}^2 + 2Oh\tilde{k}^2\alpha = 0.5\tilde{k}^2\left[1 - m^2 - \tilde{k}^2 + W_1\right] \tag{14}$$

where $Oh = \mu/(\sigma\rho r_0)^{1/2}$ is the Ohnesorge number, $W_1 = \varepsilon_0 E_r^2 r_0/\sigma B(kr_0)$ is the ratio of electrostatic pressure on the jet surface to liquid surface tension multiplied by the factor $B(kr_0) = 1 + r_0^{-1}K'_m(kr_0)/K_m(kr_0)$.[21] Here $K_m(kr_0)$ is a modified Bessel function of the mth order and m is the mode number. Substituting eq 14 into eq 13, the surface charge density, $\sigma_j^q = \varepsilon_0 E_r$, can be calculated for the corresponding wavenumber.

The length of the most unstable waves, λ, averaged over 20 images for voltage differences of 35, 40, and 45 kV, were 0.281, 0.265, and 0.216 mm, respectively, for $z_d^0 = 0.5$ cm and $d_0 = 2.24$ mm. The corresponding surface charges of the jet, σ_j^q, were determined to be 93, 95, and 98 μC/m^2.

Assuming the same surface charge density for the progeny droplets, the droplet charge was estimated as $q_d \simeq \pi d^2\sigma_j^q$. Although this relation does not give the exact progeny charge distribution, it yields reasonable approximation of the mean progeny charges and is shown by a dash-dotted line in Figure 14.

Mobility analysis was used to determine the charge of the distributed progeny drops. The governing equation for the ith progeny droplet motion is given by the droplet momentum equation

$$m_i\frac{d\mathbf{v}_d^i}{dt} = \mathbf{F}_E^i + \mathbf{F}_D^i + \mathbf{F}_q^{ij} + \mathbf{F}_g^i \tag{15}$$

where $\mathbf{F}_E^i = q_i\mathbf{E}$, is the electrostatic force due to the external electric field, $\mathbf{F}_q^{ij} = \Sigma_{i\neq j}^N[(q_i q_j \mathbf{r}_{ij})/(4\pi\varepsilon_0 r_{ij}^3)]$ is the electrostatic force due to interaction with surrounding charged droplets, and $\mathbf{F}_g^i = m_i\mathbf{g}$ is the gravitational force. The drag force acting on a droplet is given by $\mathbf{F}_D^i = 0.5C_D\pi(d_i^2/4)\rho_g(\mathbf{V}_g - \mathbf{v}_d^i)|\mathbf{V}_g - \mathbf{v}_d^i|$, where $\mathbf{v}_d^i$ is the velocity of a progeny, $\mathbf{V}_g$ is the gas velocity, and ρ_g is the gas density. The drag coefficient, C_D, is calculated as[26] $C_D^i = (24/Re_i)(1 + 0.15Re_i^{0.687})$, which fits the data of a rigid sphere coefficient to within ±5% up to $Re_i = 1000$. The use of this expression for C_D is valid because the liquid-to-air viscosity ratio is much greater than one.

Comparing the magnitude of the forces, the drag force and the force due to the external electric field are dominant and the gravitational and the mutual-interaction forces are relatively

(20) Shiryaeva, S. O.; Grigor'ev, A. I.; Levchuk, T. V.; Rybakova, M. V. *Tech. Phys.* **2003**, *48*, 527–534.
(21) Kim, O. V. Ph.D. Thesis, University of Notre Dame du Lac, 2010.
(22) de la Mora, J. F. *J. Colloid Interface Sci.* **1996**, *178*, 209–218.
(23) Loscertales, I. G.; de la Mora, J. F. *J. Chem. Phys.* **1995**, *103*, 5041–5059.
(24) Levich, V. G. *Physicochemical Hydrodynamics*, 2nd ed.; Adv. Publications Ltd.: London, 1977.
(25) Shiryaeva, S. O.; Grigor'ev, A. I.; Levchuk, T. V.; Rybakova, M. V. *Tech. Phys.* **2003**, *48*, 527–534.
(26) Schiller, L.; Naumann, A. *Ver. Deutsch. Ing.* **1933**, *44*, 318–320.

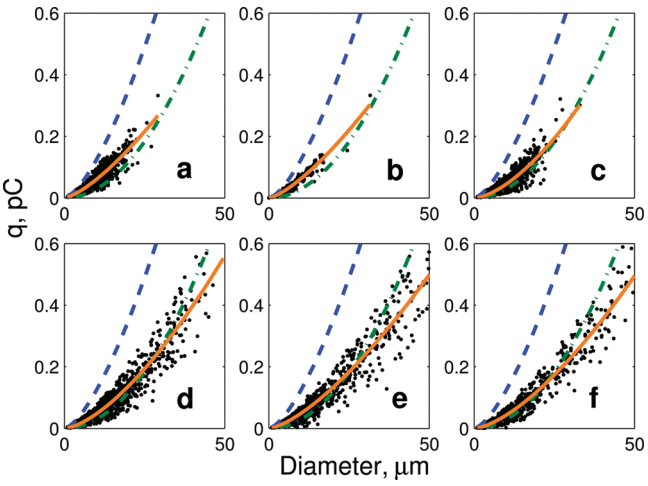

Figure 14. Charge of progeny drops produced by a 2.24 mm diameter parent drop at different applied voltage difference: (a) U_{app} = 34 kV, (f) U_{app} = 44 kV. The step between each data set is 2 kV. The points represent experimental data. Solid lines corresponds to power-law fit, $q \sim ad^n$, with $a = 1 \times 10^{-15}$–3×10^{-15} and $n \approx 1.5$. Dashed lines correspond to Rayleigh limit. Dash-dotted lines correspond to the model, $q \sim \pi d^2 \sigma_j^q$, where σ_j^q is the surface density of the jet, determined from the stability analysis of the jet nonaxisymmetric mode.

small. For drops smaller than 50 μm in diameter, the Stokes relaxation time, τ_{St}, is less than 9 μs, and the corresponding relaxation distance is smaller than ~0.2 mm. Taking into account that the axes of PDA ellipsoidal measurement volume are of 2.83 mm and of 0.28 mm, the relative change of the electric field from z_p to $z_p + L_{PDPA}$, where 0.28 mm < L_{PDPA} < 2.83 mm, is less than 2%. Thus, the field can be considered constant, and the inertial force can be considered small. Neglecting the inertial force in the left-hand side of eq 15 and $\mathbf{F}_q^{ij}$ and $\mathbf{F}_g^i$, the projection of eq 15 onto the z-axis reduces to the balance between F_{Ez}^i and F_{Dz}^i.

Using measured velocity−diameter correlations, D_{dv}, the charge of the ith progeny drop was found as $q_i = F_{Dz}^i/E_{pz}$, where F_{Dz}^i is the z-component of the drag force on the ith progeny drop and E_{pz} is the z-component of the electric field at the measurement location.

For each point of the D_{dv} domain, the corresponding value of q_i was calculated. The relation between progeny charges and their diameters, $q(d)$, is an important characteristic of the spray and is of particular interest in charged drop breakup. Here, the correlation domains measured for z_d^0 = 1 cm, U_{app} in the range from 33 to 44 kV, and at 40 mm from the tip of the corona needle were used to determine the droplet charge−diameter relation of the form $q \sim ad^n$. Figure 14 shows the measured charges of progeny droplets as a function of their diameters for 2.24 mm parent drop. Progeny−droplet Rayleigh limits, $q_R = \pi(8\varepsilon_0\sigma d^3)^{1/2}$, and the power-law fit of the experimental data are shown with dashed and solid lines, respectively. For all three studied diameters of the parent drop, n varied between 1.4 and 1.6 with the mean of 1.5. The value of n = 1.5 implies that the surface charge density is greater for smaller progenies and that the ratio of the surface stress to the electric normal stress is equal to $R_E = 8\sigma/(d\varepsilon_0 E_d^2) = 8\sigma\varepsilon_0/(d\sigma_q^2))$, where $\sigma_q = q/(\pi d^2)$.

Summary and Conclusions

In summary, the velocity, diameter, and charge measurements of progeny drops emitted by a millimeter-size parent drop under the influence of external electric and ionic fields were reported. It was demonstrated that the parent drop, undergoing breakup through the cone-jet mode, could produce either monodisperse, bimodal, or polymodal distributions of progeny droplets. The mean diameter and the mean velocity of progeny droplets were measured to be in the range from 5 to 13 μm and from 12.8 to 16.5 m/s, respectively. The charge of progenies was in the range from 2 fC to 0.6 pC.

Using mobility analysis, the relation between progeny charge and progeny diameter was found to be $q \sim d^{1.5}$ and was maintained not only for the varicose jet breakup mode (m = 0) but also for the whipping (m = 1) and ramified (m = 2) jet breakup modes. The typical nondimensional flow rates for the specific jet modes m were determined to be $1 < \tilde{Q}_{m=0} < 10^3$, $10^3 < \tilde{Q}_{m=1} < 10^5$, and $\tilde{Q}_{m=2} > 10^5$.

The influence of the applied voltage difference, the initial distance from the corona needle, and the parent drop size also were studied. It was shown that, for millimeter-size parent drops, the increase of the applied voltage difference and the decrease of the initial distance from the corona needle resulted in the exciting of higher instability modes of the jet attached to the drop apex. This shifted the diameter distribution toward submicrometer and nanometer size ranges and emitted highly polydisperse progenies, ranging from ~0.01 to 100 μm when the ramified-jet breakup mode occurred.

Larger parent drops were found to spray more polydisperse progenies than the smaller ones when experiments were conducted at the same U_{app} and z_d^0. This can be attributed to a lower E_T, higher q_f, and higher field intensities experienced by the larger drops because of their smaller deflections toward the grounded plate in the external electric field.

Acknowledgment. Partial stipend support of O.V.K. was provided through the Center for Applied Mathematics, University of Notre Dame and a research grant with The Procter and Gamble Company. We especially thank Dr. Vladimir Garstein and Dr. Alan Willey at P&G for their many technical interactions.